Spin-polarized scanning tunneling microscopy/spectroscopy study of MnAu(001) thin films

T. K. Yamada,[1,2] R. Robles,[3] E. Martinez,[4] M. M. J. Bischoff,[2] A. Vega,[4] A. L. Vázquez de Parga,[5] T. Mizoguchi,[1] and H. van Kempen[2]

[1]*Faculty of Science, Gakushuin University, 171-8588 Mejiro, Tokyo, Japan*

[2]*Institute for Molecules and Materials, Radboud University Nijmegen, Toernooiveld 1, 6525 ED Nijmegen, The Netherlands*

[3]*Department of Physics, Uppsala University, SE-75121, Uppsala, Sweden*

[4]*Department de Física Teórica, Atómica y Optica, Universidad de Valladolid, 47011 Valladolid, Spain*

[5]*Department de Física de la Materia Condensada and Instituto de Ciencia de Materiales "N. Cabrera," Universidad Autónoma de Madrid, Cantoblanco 28049, Madrid, Spain*

(Received 1 December 2004; revised manuscript received 11 March 2005; published 5 July 2005)

In this work we explore by means of spin-polarized scanning tunneling microcopy/spectroscopy (SP-STM/STS) and *ab initio* calculations the magnetic and electronic properties of thin MnAu alloyed films. The MnAu films are produced by deposition of small amounts of Au at RT on a Mn(001) surface. On the scanning tunneling microscopy images the surface of the AuMn alloy presents a $c(2\times2)$ reconstruction. From the SP-STM/STS measurements we find out that the MnAu alloy layers are coupled antiferromagnetically with the layers above and below. Comparing the result from the *ab initio* calculations with the spin-polarized measurements we found that the origin of the magnetic contrast is due to a spin-polarized peak at 0.15 eV above the Fermi level spatially placed on the Mn sites. In the calculations we also found that the magnetic moments of the Mn atoms are higher in the alloy layers than in the pure Mn films.

DOI: 10.1103/PhysRevB.72.014410 PACS number(s): 75.70.Ak, 68.37.Ef, 71.15.Mb, 73.20.At

I. INTRODUCTION

There are a limited number of studies concerning the magnetic structure of alloys composed of noble metals and antiferromagnetic materials. There are experimental and theoretical studies of the magnetism of the CuMn thin films and also concerning the $c(2\times2)$-CuMn(001) surface. The calculations for the CuMn(001) thin films identified the magnetism of Mn as the driving force for the stability of the alloy[1] and the authors tentatively suggested that the magnetic ordering of the alloy layers is determined by an indirect in-plane RKKY-type interaction due to the hybridization of the Mn *d* with the Cu *sp* electrons. In a different work, Rader *et al.*,[2] using inverse-photoemission in combination with theoretical calculations, found a high local magnetic moment for the Mn atoms in the surface alloy. A more recent calculation[3] for CuMn(001) thin films shows a ferromagnetic in-plane order and antiferromagnetic coupling between layers; a high magnetic moment for the Mn atoms in the alloy was also reported.

For the MnAu alloy, to our knowledge, there is nothing published on the magnetic structure of the MnAu thin films. However, for the bulk there are several studies concerning the magnetic structure of this alloy. $MnAu_4$ is ferromagnetic with a Curie temperature of 373 K.[4] $MnAu_3$, Mn_2Au_5, and MnAu are antiferromagnetic with Néel temperatures of 140 K, 354 K, and 513 K, respectively.[5–7] Mn_2Au presents a helical magnetic structure with a Néel temperature of 365 K.[4]

In this work we focused on the study of the $c(2\times2)$ -MnAu alloy layer grown on a Mn(001) surface by means of spin-polarized scanning tunneling microscopy/spectroscopy (SP-STM/STS). We cover clean W tips with a ferromagnetic material (iron) in order to make them sensitive to the in-plane magnetization. We found that the layers of MnAu alloy are coupled antiferromagnetically mutually. With the help of *ab initio* calculations we traced back the origin of the magnetic contrast found in the STS experiments. We also found that the magnetic moments of the Mn atoms are higher on the alloy layers than on the pure Mn films.

II. EXPERIMENTAL

All measurements were performed in an ultra-high vacuum (UHV) chamber ($\sim5\times10^{-11}$ mbar) at room temperature (RT). A STM was attached to the chamber which is equipped with molecular beam epitaxy, Auger spectroscopy, field emission spectroscopy (FES), sample heating and sputtering facilities.[8]

An Fe(001) whisker with dimensions of $\sim0.1\times0.1\times0.5$ cm^3 was used as a substrate.[9] Fe whiskers are an ideal substrate because they are extremely flat, presenting terraces up to 1 μm wide. The magnetic structure of the Fe whisker is well known[10] and the size of the magnetic domains is big enough to be sure that we are measuring with the STM in a single magnetic domain. The Fe(001) whisker was cleaned by Ar^+ sputtering and annealing cycles. After this cleaning process, less than 1% oxygen contaminants were measured by Auger spectroscopy and atomically and chemically resolved STM images.

About 7 ML of Mn (purity 99.999%) was grown on the Fe(001) whisker at 100 °C. The evaporation rate was 0.06 nm min^{-1} and the pressure was always below 4×10^{-10} mbar. After deposition, more than two Mn layers were exposed on the surface due to the layer-plus-island growth. Using atomically and chemically resolved STM images, we confirmed that there is no intermixed Fe into the Mn layers above the third Mn layer.[11] Less than 1% of con-

taminants was observed on the Mn surface. Mn layers grown on Fe(001) have a structure of body-centered tetragonal (bct) with the same in-plane lattice constant as Fe(001) and an interlayer distance of 0.165 nm.[11]

In this study, we used clean W tips as nonmagnetic tips and Fe-coated W tips as magnetic tips. A clean W tip was prepared as follows: in air, a W polycrystalline wire (purity 99.99%) with a diameter of 0.5 mm was chemically etched with 5 M KOH aq. Once in UHV the tip was sputtered using Ar^+ and heated by electron bombardment. After this treatment, a tip radius over 300 nm was measured by FES.[12] Fe-coated W tips were made by depositing 10 nm Fe on the clean W tips at RT. The Fe evaporation rate was 0.6 nm min^{-1} and the pressure remained below 2×10^{-10} mbar during deposition. We did not apply any external magnetic field to the tips.

The Au was evaporated on the Mn(001) at RT with a deposition rate of 0.15 nm min^{-1}. During the deposition the pressure was always below 3×10^{-10} mbar.

For the spectroscopy measurements, $I(V)$ curves were obtained at every pixel of a constant current topographic image by opening the STM feedback loop at a given current and voltage (set point). dI/dV curves were obtained by numerical differentiation of the $I(V)$ curves.

III. THEORETICAL METHODS

We have performed *ab initio* all-electron calculations of the electronic structure of two systems: two Mn–Au 50% alloyed monolayers on top of a Mn(001) film and the pure Mn(001) film. We have not included in the calculation the Fe(001) substrate because the STM experiments are mainly sensitive to the surface properties and the Fe–Mn hybridization effect is negligible at the surface sites if the Mn film is thick enough. The Mn films are taken large enough to simulate the semi-infinite substrate while using the supercell technique in the reciprocal space. The interlayer distance of the alloy layers is the same as that of the pure Mn substrate, as experimentally observed. For both systems this interlayer distance is 0.165 nm, while the in-plane distance is given by the Fe(001) substrate with a lattice parameter of 0.287 nm.

The calculations are performed using a scalar-relativistic version of the k-space TB-LMTO method[13,14] within the atomic-sphere approximation. This all-electron method is based on the density functional theory[15] and we have used the generalized gradient approximation for the exchange and correlation potential in the form of Perdew-Wang.[16]

In order to construct the supercell we consider enough layers of empty spheres to assure that there is no interaction between the surfaces of adjacent supercells[17] (5 monolayers of empty spheres were enough). The calculations are performed using an increasing number of k points in the irreducible Brillouin zone (integrations are done with the tetrahedron technique) until the total energy does not change within our convergence error (10^{-5} eV). A total number of 98 k points fulfills this requirement.

IV. RESULTS AND DISCUSSION

The Au–Mn alloy was produced by evaporation of small amounts of Au on the surface of 7 ML of Mn grown on the surface of an Fe(001) whisker. We will first discuss the electronic and magnetic characteristics of the Mn(001) films. Scanning electron microscopy with polarization analysis results suggested that for films thicker than three layers the ferromagnetic Mn(001) sheets couple antiferromagnetically among each other.[18] In a recent publication Yamada *et al.*[19] showed that above the third layer each ferromagnetic Mn layer, whose magnetization direction is in-plane, couples antiferromagnetically with the Mn layer above and below. The antiferromagnetic coupling between layers produces the existence of different magnetic domains on the surface every time the thickness of the Mn film changes, i.e., every time a surface step is crossed. The body-centered-tetragonal (bct) Mn(001) surface has two d_{z^2} surface states that are responsible for the magnetic contrast observed in the SP-STM.[19] Therefore we used this well-known and well-characterized surface to check the sensitivity of our Fe-coated W tips to the in-plane surface magnetization.

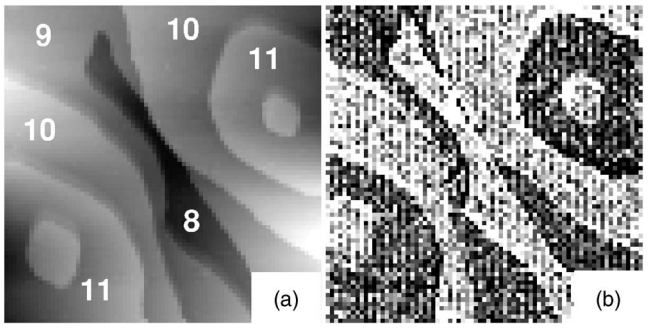

FIG. 1. (a) The 100×100 nm^2 STM topography of 9.5 ML of Mn grown on an Fe(001) whisker. The numbers denote the local Mn thickness. (b) The dI/dV map at +0.2 V showing the magnetic contrast between different Mn layers.

Figure 1(a) shows an example of the surface topography after the deposition of 9.5 ML of Mn. In the image it is possible to identify five different Mn layers, from 8 to 12, a clear indication of a quasi-layer-by-layer growth mode.[11] In STM the tunneling probability depends on the local density of states (LDOS) of tip and sample in an energy window determined by the bias voltage applied between them. If the STM tip used in the experiment is covered with ferromagnetic material, then the tunneling probability also depends on the relative orientation between the magnetizations of sample and tip.[20]

Taking $I(V)$ curves in every pixel of the topographic image it is possible to construct an image of the value of the differential tunneling conductance (dI/dV) at certain bias voltage. Figure 1(b) shows the dI/dV map at +0.2 V constructed in this way. From previous studies[19,11] we know that the LDOS of the Mn layers does not change from layer to layer for films thicker than 4 ML. Depending on the Mn local thickness the magnetization of the sample is parallel (antiparallel) to the one of the tip, and therefore the tunneling probability is higher (lower), giving the contrast observed in Fig. 1(b). Using these Mn layers we can check the sensitivity of our Fe covered tips to the in-plane sample magnetization.

Figure 2 shows STM images obtained on the surface of the sample after the deposition at RT of 0.4 ML (a) and 0.9

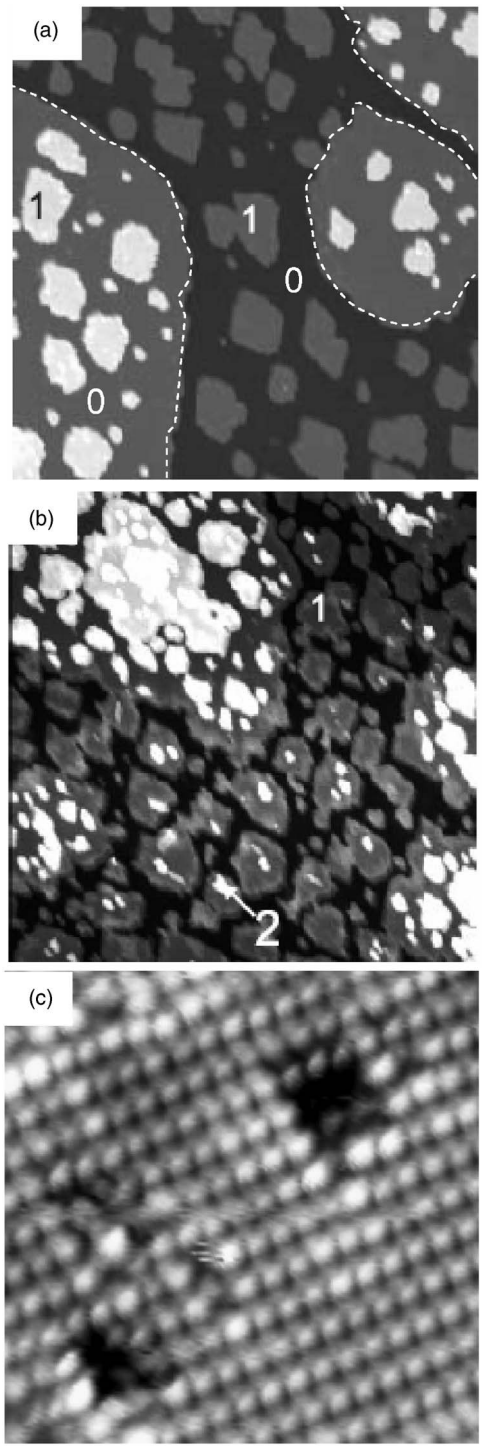

FIG. 2. (a) The 100×100 nm^2 STM topographic image obtained on a Mn surface covered by 0.4 ML of Au. The white broken lines mark the position of the original Mn steps. (b) The 100×100 nm^2 STM topographic image obtained on a Mn surface covered by 0.9 ML of Au. (c) 6.6×6.6 nm^2 atomic resolved image obtained on a 2.2 ML Au film deposited at RT showing the $c(2\times2)$ surface reconstruction and several defects.

ML (b) of Au on a 7 ML Mn(001) film. A close inspection of the surface [Fig. 2(c)] reveals a $c(2\times2)$ structure that covers all the sample surface. This surface reconstruction appears after the deposition of 0.5 ML of Au on the surface and exists on the surface upon deposition of up to 3 ML of Au. Figure 2(a) is taken after deposition of 0.4 ML of Au. The big islands present on the image (marked with white broken lines) correspond to Mn islands already present before the deposition of the Au. The areas marked with "0" correspond with the level of the original Mn surface. Figure 2(b) is taken after the deposition of 0.9 ML of Au. The growth is almost layer by layer; the second layer (marked as 2 in the image) is starting to develop before the first layer (marked as 1 in the image) is completed. For thicker Au films the $c(2\times2)$ reconstruction disappears and it is replaced by a $p(1\times1)$ due to the growth of pure Au layers.

Several studies concerning the bulk magnetic structure of different AuMn alloys[4–7] prove the existence of bulk alloys of Au and Mn. On the other hand, experimental studies on Mn/Au(001),[21] Mn/Ag(001),[22] and Mn/Cu(001) (Refs. 23 and 24) show that in all cases the Mn forms a $c(2\times2)$ surface alloy with the noble metals. In the case of one monolayer thick epitaxial $c(2\times2)$ MnCu surface alloy film on Cu(100), the Mn atoms show an unusual buckling relaxation[1] that is the origin of the structure that we observe in the STM measurements. The details of the geometric structure of the films are described elsewhere.[25]

As mentioned before, in SP-STM experiments the information concerning the relative orientation of the sample magnetic domains appears as small changes in the intensity of the differential tunneling conductance (dI/dV) measured in the different magnetic domains. Therefore, in order to be able to use this technique to study the magnetic properties of the MnAu alloy films, it is important to carefully characterize the dI/dV curves measured with a clean W tip. In fact, we have to be sure that the LDOS of the sample does not change from layer to layer in the alloy or from one area to the other on the surface. For this reason we first performed spectroscopic measurements using a clean W tip.

Figure 3(a) shows a representative STM topography of the surface after deposition of 0.6 ML of Au on the Mn(001) surface at RT. As mentioned before the surface presents a $c(2\times2)$ reconstruction in all the levels exposed. Figure 3(b) shows the dI/dV curves (solid lines) measured on the substrate (black line) and the first layer (gray line) of the image shown in panel (a) with a clean W tip. It is clear that the curves measured in every layer exposed on the surface present the same shape and amplitude in the voltage range explored in our experiments.

The energy position of the features in the sample LDOS is difficult to estimate from the dI/dV curves, due to the voltage-dependent exponential background. In addition the features appear as shoulders in the dI/dV curves, making it more difficult to determine their exact energy position. In order to circumvent these problems we normalized the dI/dV curves to reduce the influence of the exponential background.

For metallic samples it has been proposed that the best way to recover the sample density of states from the dI/dV curves is normalizing them by their fit to a tunneling probability function ("T") (Ref. 26) that is given by the following expression:

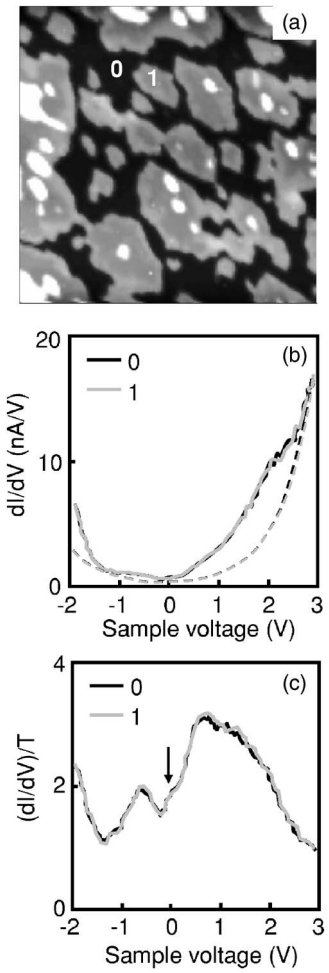

FIG. 3. (a) The 40×40 nm^2 STM image taken after the deposition of 0.6 ML of Au on the Mn(001) surface at RT. "0" denotes the substrate and "1" denotes the islands. (b) The dI/dV curves measured simultaneously with the image shown in panel (a) (solid lines). The exponential background fit for both curves is shown with dashed lines. The black curves correspond to the data measured on the substrate (0) and the gray curves correspond to the ones measured on the islands (1). (c) The normalized tunneling conductance using the exponential fitting shown in panel (b). Three clear contributions to the tunneling conductance can be distinguished in the spectra.

$$T = a_t \exp\left[-2S\left[\frac{2m}{\hbar^2}\left(\bar{\phi}-\frac{V}{2}\right)\right]^2\right] + a_s \exp\left[-2S\left[\frac{2m}{\hbar^2}\left(\bar{\phi}+\frac{V}{2}\right)\right]^2\right]. \quad (1)$$

The first (second) term of T describes the tunneling from the tip (sample) Fermi level to the unoccupied sample (tip) states. a_t and a_s are proportionality coefficients related to the tip-surface effective contact area and are proportional to the tip and sample DOS at the Fermi level, respectively. $\bar{\phi}$ is the average of tip and sample work function, S is the tip sample distance, and m is the electron mass. To use this normalization procedure it is necessary to fit the exponential background accurately. Therefore it is necessary to have the $I(V)$ curves measured over a wide voltage range as shown in Fig. 3 where the $I(V)$ curves have been measured between −2 V up to +3 V.

In Fig. 3(b) we plot the exponential background fit (dashed lines) for the dI/dV curves (solid lines). The dI/dV curves deviate from the exponential background. This is a clear indication of the contribution to the differential tunneling conductance from well-defined features of sample LDOS. Using the exponential background fit ("T"), we normalize the dI/dV curves to get a precise determination of the energy position of the different features present in the dI/dV curves. As shown in Fig. 3(c) the normalized conductance curves obtained in the substrate and first layer are also identical and present three clear features: a peak at -0.6 ± 0.1 V, a small feature marked with a black arrow at $+0.1\pm0.1$ V, and a broad peak at $+0.9\pm0.1$ V. All these peaks are present in all the curves measured with different clean W tips. The amplitude of all these features is identical in all the layers exposed when they are measured with a clean W tip. These curves are very different from the ones measured in the Mn(001) surface,[19] therefore we conclude that these curves are representative of the sample DOS for the AuMn surface alloy.

In the dI/dV curves obtained with the Fe covered tips we found the same spectral features as in the curves measured with the clean W tips. A careful analysis reveals that in the dI/dV curves measured with the Fe covered tip the intensity of the small peak at +0.1 V [marked with an arrow in Fig. 3(c)] changes when the tip goes from one terrace to the other. In the following we will only plot the dI/dV curves in an energy range of ±0.4 V around the Fermi level to make these changes in intensity more visible.

Figure 4(a) shows a STM image after a deposition on 0.7 ML of Au on the Mn(001) surface. The broken white line marks the approximate position of the original Mn step. Therefore the upper right corner (labelled "*odd*") and the rest of the image (labelled "*even*") correspond to different terraces of the Mn film [see Fig. 1(a)]. Figure 4(b) shows an image constructed with the value of the differential conductance (dI/dV) at +0.1 V for the individual $I(V)$ curves measured in every pixel of the image shown in panel (a). The magnetic contrast between the terraces and the islands is inverted after crossing the Mn step. For the terrace labelled *odd* the islands are dark and the terrace is bright. On the contrary in the terrace labelled *even* the islands are bright and the terrace is dark. In panels (c) and (d) we show the dI/dV curves measured in the *even* and *odd* areas of the image for the substrate (solid line) and islands (dashed line). This result indicates that the magnetic structure of the MnAu alloy is coupled with the magnetic structure of the Mn(001) film underneath.

Figure 5(a) shows a STM image of the surface of 1.1 ML of Au deposited on Mn(001) surface. In this image there are four different levels exposed due to the quasi-layer-by-layer growth mode. In this surface there are present three different thicknesses of the MnAu alloy marked in the image as "1," "2," and "3." In Fig. 5(b) we present a narrow energy range of the dI/dV curves taken in three different areas mentioned above. The curves are identical in the energy range measured and the only difference appears around +0.1 V. The intensity

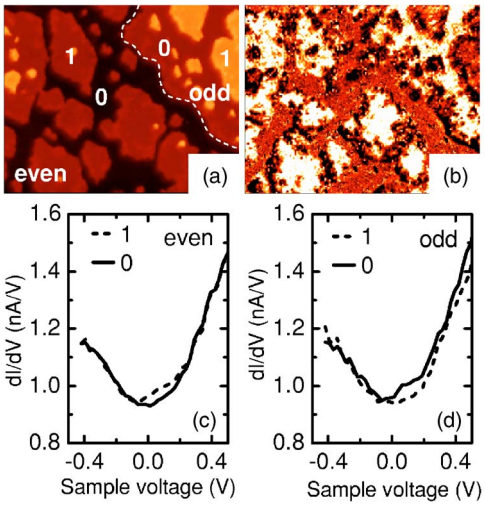

FIG. 4. (Color online) (a) The 50×37 nm^2 STM image taken after deposition of 0.7 ML of Au on the Mn(001) surface. Three different levels are seen in the image. The white broken line marks the approximate position of the original Mn step. The odd and even areas correspond to different terraces of the Mn film. On the image the substrate is marked with "0" and the islands with "1." (b) The image constructed with the value of the dI/dV at +0.1 V measured in every pixel of the image shown in (a). (c) The averaged dI/dV curves measured on the substrate marked as "0" on panel (a) (continuous line) and on the islands marked as "1" on panel (a) (broken line) of the area marked as even on panel (a) (lower left corner). (d) The averaged dI/dV curves measured on the substrate marked as "0" on panel (a) (continuous line) and on the islands marked as "1" on panel (a) (broken line) of the area marked as odd on panel (a) (upper right corner).

of the differential tunneling conductance oscillates with the thickness. It is high for areas "1" and "3" (solid and dotted curves, respectively) and low for area "2" (dashed curve). This result indicates a nonferromagnetic coupling between layers in the MnAu ordered alloy.

In order to fully understand these results we have performed *ab initio* all-electron calculations of the electronic structure of two systems: two Mn–Au 50% alloyed monolayers on top of a Mn(001) film and the pure Mn(001) film. For both the pure Mn(001) film and the two Mn–Au 50% alloyed monolayers on top of the Mn(001) film we obtain the

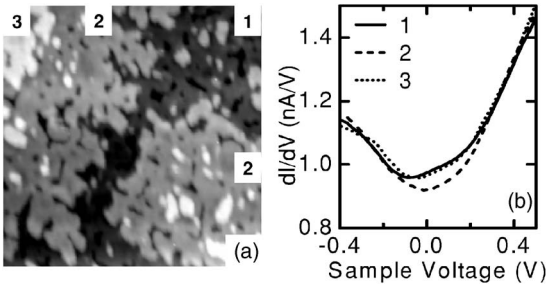

FIG. 5. (a) The 80×80 nm^2 STM image taken after deposition of 1.1 ML of Au on the Mn(001) surface. Four different levels are seen in the image. (b) The dI/dV curves measured with Fe covered W tips on terraces marked 1 (solid curve), 2 (dashed curve), and 3 (dotted curve).

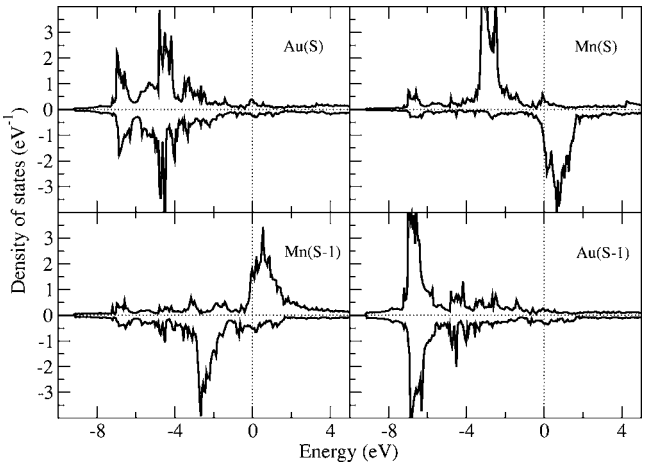

FIG. 6. The spin-resolved DOS for the Mn and Au atoms on the Mn—Au alloyed layers for the surface layer (S) and the subsurface layer (S-1).

layered antiferromagnetic structure (LAF) as experimentally observed. Although the presence of Au does not modify the magnetic coupling in the system, quantitative differences in the magnetic moments of the surface Mn atoms exist as a consequence of the change of the local chemical environment.

In Fig. 6 we plot the calculated spin resolved DOS for the Mn and Au sites of the first two layers of the MnAu alloy on top of 7 ML of Mn. The change of sign of the spin polarization at the different (001) planes is characteristic of the LAF configuration. Au is a noble metal, thus the Mn–Au hybridization is small and for this reason the spin polarization of the Au atoms is negligible. The spin polarization of the Mn atoms is clear and also the oscillation in the sign from layer to layer. This oscillation in the spin polarization on the Mn sites is the origin of the contrast found in the dI/dV curves measured with the Fe covered tips.

To get a better understanding of the role played by the Mn and the Au atoms on the magnetic structure of the thin MnAu alloy film, we calculated the number of electrons per atomic site for the s, p, and d bands in the pure Mn(001) films and in the 2 ML thick MnAu alloy. The result is shown in Table I for the Mn and Au atoms. For the theoretical calculation of

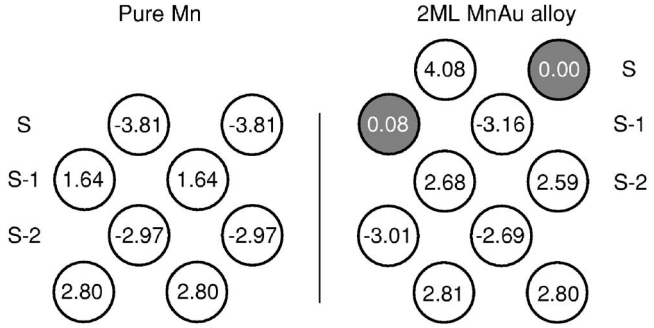

FIG. 7. (a) The local magnetic moments of the Mn atoms for the first four layers of a pure Mn(001) film. (b) The local magnetic moments for the Mn (empty circles) and Au atoms (gray circles) for the 2 ML of MnAu alloy on a Mn(001) film.

TABLE I. This table shows the electron population in the *s*, *p*, and *d* bands for the pure Mn(001) layers and for the 2 ML thick MnAu alloy as well as the value of the magnetic moment in Bohr magnetons.

	Mn(001)					MnAu c(2×2)			
	s	*p*	*d*	μ		*s*	*p*	*d*	μ
Mn(S)	0.62	0.49	5.46	−3.81	Mn(S)	0.58	0.51	5.45	4.08
					Au(S)	0.87	0.50	9.12	0.00
Mn(S-1)	0.67	0.84	5.68	1.64	Mn(S-1)	0.67	0.85	5.67	−3.17
					Au(S-1)	0.92	0.90	9.04	0.08
Mn(S-2)	0.67	0.81	5.49	−2.97	Mn(S-2)	0.65	0.82	5.58	2.68
					Mn(S-2)	0.65	0.81	5.58	2.59

the alloy layers, it was assumed that the S-2 layer is the first one composed only of Mn. In this layer there are two inequivalent Mn atoms. For one of them all the second nearest neighbors are Mn and for the other some are Au. Comparing the occupancy of the *d* bands for the Mn atoms in the pure Mn(001) layers and in the 2 ML thin MnAu alloy we found that this is almost identical for every layer. This is a clear indication of the low hybridization between the Mn and the Au atoms.

In Fig. 7 we plot the magnetic moment distribution obtained in both systems. Mn atoms at the Mn–Au surface alloy have larger magnetic moments than the surface atoms of the pure Mn(001) film. Moreover, the local magnetic moments of the Mn atoms of the first three layers are different in both systems. Due to the small Mn–Au hybridization, the Mn atoms close to the Au atoms in the Mn–Au alloy behave as if they were less coordinated than the Mn atoms of the pure Mn(001) system. This situation is more extreme for the surface Mn atoms in the MnAu alloy where they are closer to the magnetic saturation limit. As mentioned earlier, the spin polarization of the Au atoms is negligible as expected. The magnetic moments found in our calculation for the Mn and Au atoms in the MnAu alloy are similar to the values found for MnCu alloy.[2] It has been claimed that the large magnetic moment of the Mn atoms is the basic source for the formation and stability of the surface alloys.[1]

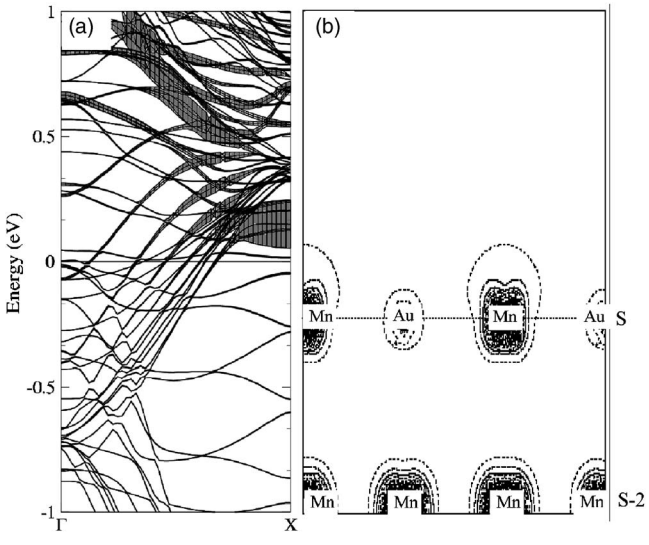

FIG. 8. (a) The majority bands in the Mn site at the surface of the alloy. (b) The isocharge density distribution in an energy window of 0.25 eV above the Fermi level layers. The dashed line indicates the boundary between vacuum and the bulk.

In Fig. 8 we plot the projection of the majority bands (a) in the Mn site at the surface layer of the alloyed system. The thickness of the bands is proportional to the percentage of the atom in this band. So, if the band is very thick, it means that it is due mainly to this atom. A broad band can be observed at 0.15 eV above the Fermi level close to the *X* point of the Brilluoin zone. Thus we can identify the peak at 0.1 eV in our dI/dV curves as coming from the Mn atoms at the surface. In panel (b) of Fig. 8 we plot the isocharge density distribution in an energy range of 0.25 eV above the Fermi level. This is the energy range where differences in the intensity have been found in the dI/dV curves measured in this system. In this plot only the atoms of the surface (S) and the second layer below the surface (S-2) are visible. Due to the geometric structure in this plot the atoms of the subsurface layer (S-1) do not lay in the same plane. As mentioned before, for the alloy layers the S-2 layer is the first layer composed only by Mn.

In conclusion, we have studied the magnetic and electronic structure of the MnAu alloy grown on a Mn(001) surface by means of spin-polarized scanning tunneling experiments and *ab inito* all-electron calculations. The MnAu films are produced by deposition of small amounts of Au at RT on a Mn(001) surface. On the scanning tunneling microscopy images, the surface of the MnAu alloy presents a $c(2\times2)$ reconstruction. By means of SP-STS measurements we found an in-plane magnetization with a ferromagnetic coupling between the Mn atoms in the same layer and a layered antiferromagnetic structure. The calculated density of states close to the Fermi level is dominated by a spin-dependent peak at +0.15 eV that is located mainly at the Mn atomic sites. This peak is the origin of the contrast in the SP-STS images. The hybridization between Mn and Au atoms is negligible and a very high magnetic moment of the Mn atoms on the MnAu alloy is found, especially at the surface.

ACKNOWLEDGMENTS

ALVP acknowledges the financial support by the Spanish Ministry of Education (MEC) through Project No. FIS2004-

01026. RR and AV aknowledge financial support by the Spanish Ministry of Science and Technology through Project No. MAT2002-03142. TKY acknowledges the Grant-in-aid for JSPS fellows. The authors thank Dr. D.T. Pierce for supplying the Fe whiskers.This work was supported by the Stichting voor Fundamenteel Onderzoek der Materie (FOM), which is funded by the Nederlandse Organisatie voor Wetenschappelijk Onderzoek (NWO).

[1] M. Wuttig, Y. Gauthier, and S. Blügel, Phys. Rev. Lett. **70**, 3619 (1993).
[2] O. Rader, W. Gudat, C. Carbone, E. Vescovo, S. Blügel, R. Kläsges, W. Eberhardt, M. Wuttig, J. Redinger, and F. J. Himpsel, Phys. Rev. B **55**, 5404 (1997).
[3] M. Eder, J. Hafner, and E. G. Moroni, Phys. Rev. B **61**, 11492 (2000).
[4] S. Abe, M. Matsumoto, H. Yoshida, S. Mori, T. Kanomata, and T. Kaneko, J. Magn. Magn. Mater. **104–107**, 2059 (1992).
[5] K. Sato, T. Hirone, H. Watanabe, S. Maeda, and K. Adachi, J. Phys. Soc. Jpn. **17**, 160 (1962).
[6] M. Matsumoto, S. Abe, H. Yoshida, S. Mori, T. Kanomata, and T. Kaneko, J. Magn. Magn. Mater. **104–107**, 2061 (1992).
[7] M. Matsumoto, T. Kaneko, and K. Kamigaki, J. Phys. Soc. Jpn. **25**, 631 (1968).
[8] T. K. Yamada, M. M. J. Bischoff, T. Mizoguchi, and H. van Kempen, Appl. Phys. Lett. **82**, 1437 (2003).
[9] R. N. Gardner, J. Cryst. Growth **43**, 425 (1978).
[10] R. Schäfer, R. Urban, D. Ullmann, H. L. Meyerheim, B. Heinrich, L. Schultz, and J. Kirschner, Phys. Rev. B **65**, 144405 (2002).
[11] T. K. Yamada, M. M. J. Bischoff, T. Mizoguchi, and H. van Kempen, Surf. Sci. **516**, 179 (2002).
[12] G. J. de Raad, P. M. Koenraad, and J. H. Wolter, J. Vac. Sci. Technol. B **17**, 1946 (1999).
[13] O. K. Andersen and O. Jepsen, Phys. Rev. Lett. **53**, 2571 (1984).
[14] O. K. Andersen, Z. Pawlowska, and O. Jepsen, Phys. Rev. B **34**, 5253 (1986).
[15] P. Hohenberg and W. Kohn, Phys. Rev. **136**, B864 (1964); W. Kohn and L. J. Sham, Phys. Rev. **140**, A1133 (1965).
[16] J. P. Perdew and Y. Wang, Phys. Rev. B **45**, 13244 (1992).
[17] M. A. Khan, J. Phys. Soc. Jpn. **62**, 1682 (1993).
[18] D. A. Tulchinsky, J. Unguris, and R. J. Celotta, J. Magn. Magn. Mater. **212**, 91 (2000).
[19] T. K. Yamada, M. M. J. Bischoff, G. M. M. Heijnen, T. Mizoguchi, and H. van Kempen, Phys. Rev. Lett. **90**, 056803 (2003).
[20] M. Bode, Rep. Prog. Phys. **66**, 523 (2003).
[21] W. Kim, S.-J. Oh, J. Seo, H. G. Min, S. C. Hong, and J.-S. Kim, Phys. Rev. B **65**, 205407 (2002).
[22] P. Schieffer, C. Krembel, M.-C. Hanf, G. Gewinner, and Y. Gauthier, Phys. Rev. B **65**, 235427 (2002).
[23] H. P. Noh, T. Hashizume, D. Jeon, Y. Kuk, H. W. Pickering, and T. Sakurai, Phys. Rev. B **50**, 2735 (1994).
[24] R. G. P. van der Kraan and H. van Kempen, Surf. Sci. **338**, 19 (1995).
[25] T. K. Yamada, Ph.D. thesis, Radboud University, Nijemegen, The Netherlands, 2005; http://webdoc.ubn.ru.nl/mono/y/yamada_t/studofsps.pdf.
[26] V. A. Ukraintsev, Phys. Rev. B **53**, 11176 (1996).